DIRECT NUMERICAL SIMULATION OF THE INTERACTION OF A WALL-ATTACHED CUBE WITH A TURBULENT BOUNDARY LAYER

C. Diaz Daniel, S. Laizet and J. C. Vassilicos

Department of Aeronautics, Imperial College London, United Kingdom

c.diaz-daniel13@imperial.ac.uk

Abstract

A wall-attached cube immersed in a turbulent boundary layer is studied by means of Direct Numerical Simulations (DNS) at a Reynolds number $Re_H = 3000$, based on the cube height and the free-stream velocity U_∞. The main features of the flow around the cube are in good agreement with previous experimental and numerical data, even if in those studies the cube was immersed in a turbulent channel. In the near-field, downstream of the cube, a vortex shedding with a Strouhal number $St = 0.14$ can be identified in the energy spectra, which can no longer be detected when moving further downstream. However, far away from the boundary layer, a low frequency peak with $St = 0.05$ can be observed at long streamwise distances $x > 20 - 30H$. In order to investigate the origin of this low-frequency peak, the cube was simulated at $Re_H = 750$ and immersed in a laminar boundary layer, which revealed further information about the mechanisms of the unsteady flow structures.

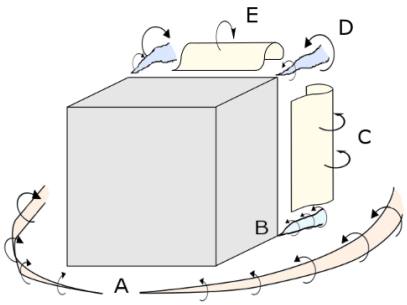

Figure 1: Sketch of the different flow features around the cube: A) horseshoe vortex, B) base vortices, C) lateral shedding, D) Tip vortices, E) Top vortex.

1 Introduction

The turbulent flow around a wall-attached solid cube represents an interesting and complex problem from a fundamental point of view. As well, it is a simple model for the interaction between a boundary layer and complex bodies immersed in it. The three-dimensionality of the flow and the cube's finite-length generate distinctive flow features that have been sketched in Figure 1 and can be hinted by visualising the meanflow streamlines from our simulation in Figure 2.

Castro and Robins (1977) were among the first ones to perform an exhaustive experimental study of this problem, comparing the effect of uniform and sheared turbulent incoming streams. Since then, this flow configuration has been revisited many times using experiments and computational simulations (for instance, see Martinuzzi and Tropea (1993), Meinders et al. (1999), Yakhot et al. (2006), Porteous et al. (2014)). Recent DNS of wall-attached cylinder by Vinuesa et al. (2015) has also shown evidence that upstream flow conditions (laminar versus turbulent) can have a strong effect on the structure of the turbulent wake of wall-attached bodies, while they suggest that the shedding frequency remains unchanged.

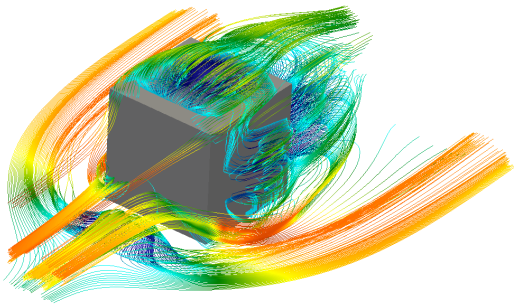

Figure 2: Meanflow streamlines around the solid cube from current simulation.

Solid objects immersed in boundary layers can modify the flow properties in a noticeable way even with a small blockage ratio and their turbulent wake introduces a momentum loss which results in a rapid increase of the boundary layer thickness. Moreover, despite the small relative size of these solid objects, their effect on the spectral signature of the flow can persist far downstream. This article studies the free-stream signature of a wall-mounted cube, focusing on the low-frequency peak found in the energy spectra at

high distances from the wall and cube position. Firstly, the computational results are presented, validating the near-field flow statistics using previous author's data (Martinuzzi and Tropea, 1993; Yakhot et al., 2006). After that, the energy spectrum peak is described and its evolution and origin are investigated.

2 Computational method

The results presented in this study have been obtained from high fidelity Direct Numerical Simulations of a zero-pressure gradient turbulent boundary layer (TBL), with and without a solid cube immersed in the computational domain. The flow solver, Incompact3d (Laizet and Lamballais, 2009), is a 6th-order finite difference code, with a spectral treatment for the pressure equation and a semi-implicit time advancement for the viscous terms. Current simulations have been performed with $4097 \times 513 \times 256$ cells in a domain of size $320 \times 27 \times 10$ H, where H is the cube height. The local Reynolds number of the TBL covers the range $Re_\theta = 270 - 2200$, based on the momentum thickness θ and free-stream velocity U_∞. The computational domain is stretched in the wall normal direction and the resolution, in wall viscous units (at $Re_\theta = 1470$) is: $\Delta x^+ = 10.2$, $\Delta z^+ = 5.1$, $\Delta y^+ = 0.42$ at the wall and $\Delta y^+ = 108.8$ at the top of the domain. The stretching function, described in Laizet and Lamballais (2009), allows more flexibility than the one based on Chebyshev's polynomials, traditionally used in spectral flow solvers. The spacing of the first point was controlled to be not necessarily too small, which permitted higher wall-normal resolution within $y^+ = 1 - 550$ than the Chebyshev's stretching.

At the inlet, a Blasius laminar boundary layer profile is prescribed and transition to a turbulent state is triggered via the random-forcing method described in (Schlatter and Örlü, 2012). A streamwise convective equation is solved at the outlet and a no-slip condition is imposed on the bottom wall. Periodic boundary conditions are used in the spanwise direction, modelling an infinite array of cubes, and an homogeneous Neumann condition is imposed at the top boundary. The cube is located at the streamwise position $x/H = 72$, where the local boundary layer Reynolds is $Re_\theta = 750$. It is modelled via an immersed boundary method (IBM), based on a volume forcing to ensure zero velocity at the cube surface. The Reynolds number based on $H = 0.42\delta$, where δ is the local boundary layer thickness, is 3000. The blockage ratio, based on the frontal area of the obstacle and the total area occupied by δ, is $\sigma = 4.2\%$. The statistics presented in this study have been averaged over $T = 1000H/U_\infty$ ($T^+ = 5500$), after an initial period of $T \approx 1350H/U_\infty$.

3 Results

Mean-flow features in the near-cube region

The mean flow features are compared with previous authors' experimental and simulation data (Martinuzzi and Tropea, 1993; Yakhot et al., 2006). In those studies, the Reynolds number Re_H is similar, but the cube is immersed in a turbulent channel. The flow streamlines in Figures 3 and 4 show the time averaged structures around the cube. In the centre plane $z = 0$, the stagnation point A is located at $y/H = 0.65$, the reattachment point E at $x/H = 2.5$, the front vortex C has its centre at $x/H = 0.48$ and the horizontal location of the rear recirculation centre D is $x/H = 1.4$. Those spatial positions are in good agreement with the numerical results in Yakhot et al. (2006), with differences of less than 3%. On the other hand, the location of the top recirculation bubble B, $x/H = 0.65$ and $y/H = 1.13$, and the vertical position of the rear recirculation D, $y/H = 0.85$, have a 10-15% relative error with respect to the values found in Yakhot et al. (2006). This can be explained by the different top boundary condition, since the channel configuration constraints the flow in the vertical direction.

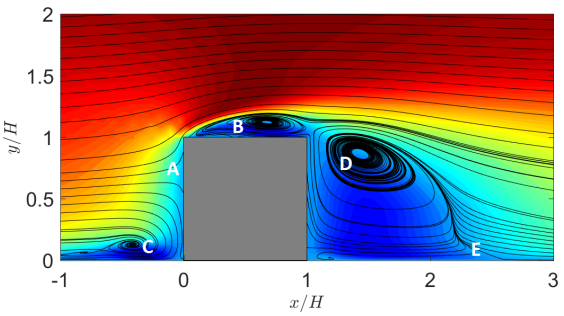

Figure 3: Mean velocity streamlines in the spanwise plane $z = 0$. Coloured contours by velocity magnitude (from 0, blue, to $1.1U_\infty$, red).

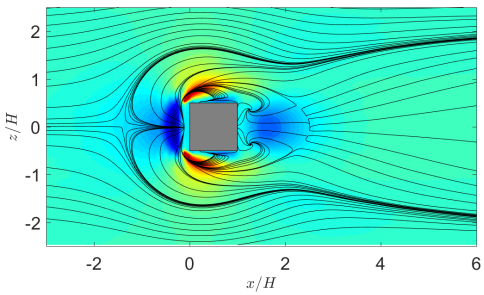

Figure 4: Mean velocity streamlines in the wall-normal plane $y/H = 0.0045$. Coloured contours by streamwise velocity (from $-0.1U_\infty$, blue, to $0.2U_\infty$, red).

Periodic boundary conditions in the spanwise direction are modelling an infinite array of cubes and one can average the flow variables in the z direction to estimate the cube effect on the boundary layer statis-

tics. The cube increases the Reynolds number based on the span-averaged momentum thickness, Re_θ, by a constant, as shown in Figure 5, which can be directly related to the drag coefficient of the cube. Having obtained $\Delta Re_\theta = 103$, the drag coefficient can be computed as $C_d = 2\Delta\theta L_z/H^2 = 0.7$, which is in good agreement with the different experimental results reported by Wang et al. (2012). Differences in drag coefficient with the experiments of Martinuzzi and Havel (2004) ($C_d \approx 0.95$) can be due to the different incoming flow conditions (in their study, a Blasius profile was prescribed to a boundary layer with $\delta/H = 0.07$), which can affect the cube wake characteristics. Moving downstream, the span-averaged velocity profiles recover a canonical state for the inner and buffer regions of the TBL and the influence of the cube is mostly concentrated on the inertial and wake layers . The span-averaged turbulent fluctuation profiles, presented in Figure 6, at $Re_\theta = 1000$, $30H$ downstream of the cube, show a significant increment between $y^+ \approx 80$ and $y^+ \approx 300$, while the inner part of boundary layer remains unaltered. Thus, the effect of the immersed cube on the the span-averaged turbulence statistics is mostly concentrated around its upper edge, located at $y^+ \approx 130$.

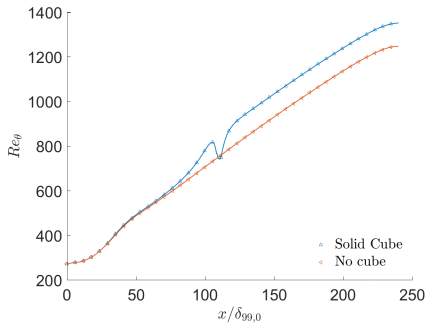

Figure 5: Effect of the cube on the span- averaged momentum thickness.

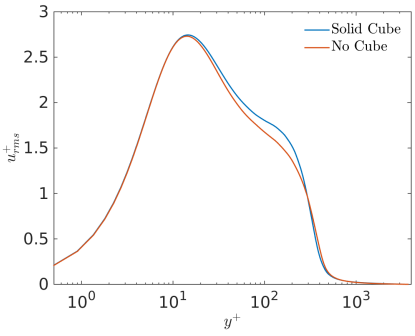

Figure 6: Effect of the solid cube in the span-averaged streamwise fluctuations, at $Re_\theta = 1000$.

Energy spectra inside the boundary layer

In the near-field flow around the cube, for $y < H$, rear and lateral recirculations shed unsteady vortices, producing a dominant peak in the velocity spectra. Previous studies have reported a shedding frequency with a Strouhal number $St = fH/U_\infty = 0.08 - 0.15$ (Yakhot et al., 2006; Porteous et al., 2014; Martinuzzi and Havel, 2004). In our simulation, close to the rear wall of the obstacle ($x = 4.7H, y = 0.73H, z = 0$), it is possible to identify a peak in the turbulence spectra with $St = 0.14$ as seen in Figure 7. The peak frequency lies within the range of values found in the literature and is in good agreement with the empirical correlation of Wang et al. (2012), based on experimental results. Further downstream, the peak in the energy spectra of the streamwise component u is masked by the boundary layer turbulence and it is not easily detected inside δ (see Figure 7 for $x = 36H$). The spectra of the spanwise component w also presents a peak with $St = 0.14$ which is shown in figure 8, confirming that the velocity fluctuations created by the cube are three-dimensional. While the magnitude of this peak decreases further downstream, it is still noticeable at $y/H = 36$, as the background spanwise fluctuations of the boundary layer are less intense than the streamwise ones.

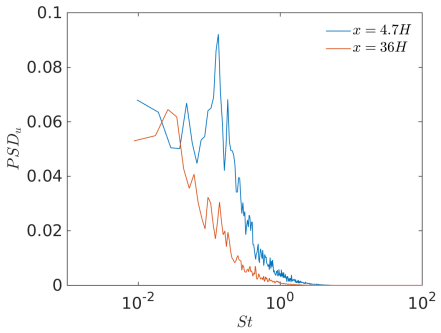

Figure 7: Energy spectra of streamwise velocity from the cube simulation, at $y = 0.73H$ and $z = 0$. Comparison at $x = 4.7H$ and $x = 36H$ downstream of the cube (points P and P' in Figure 9).

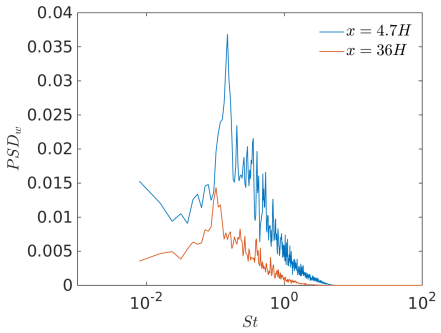

Figure 8: Energy spectra of spanwise velocity from the cube simulation at $y = 0.73H$ and $z = 0$. Comparison at $x = 4.7H$ and $x = 36H$ downstream of the cube (points P and P' in Figure 9).

Energy spectra outside the boundary layer

In the free-stream, an array of virtual probes recorded the velocity signal as a function of time at different streamwise positions and same distance from the wall, $y/H = 4.7$, as sketched in Figure 9. In this region, the flow statistics have small variations in the spanwise direction and, thus, the frequency spectra have been averaged over 16 equally-spaced spanwise positions to improve statistical convergence. Far away from the boundary layer (at least $y/H = 3-4$ from the wall), a sharp peak with Strouhal number $St = 0.05$ is found in the turbulence spectra for large distances downstream of the cube, around $x/H > 30$ (Figure 10). The peak magnitude is low since this position is far from the turbulent region, but it is over 5 times higher than the boundary layer background level.

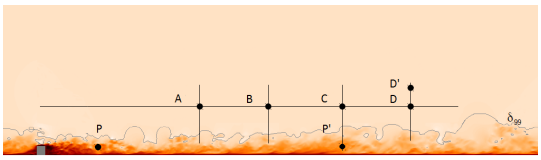

Figure 9: Probe positions for the frequency spectra. Points P, P': inside boundary layer, $x/H = 4.7, 36$, $y/H = 0.7$. Points $A - D$, free-stream far-field, $y/H = 4.7$ and $x/H = 20, 28, 36, 45$; D' at $y/H = 6.5$, $x/H = 45$.

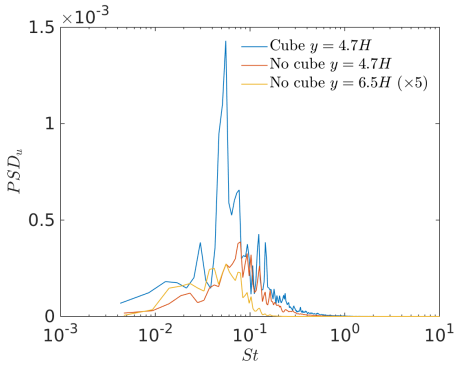

Figure 10: Span-averaged energy spectra of the streamwise component u. Comparison with and without cube at $x/H = 36$, $y/H = 4.7$ from the cube position.

According to Philips (1955), the boundary layer turbulence motion propagate to the free-stream as irrotational fluctuations and the energy spectra of the unperturbed TBL decays as $E_{11}(k_1, y) = E_{11}(k_1, \delta)\exp(-2k_1 y)$ out of the turbulent region. Applying the Taylor hypothesis, the frequency f is directly proportional to the wave-number k_1 by a factor U_∞. The frequencies in the broad peak of the energy spectra in the TBL's free stream therefore decrease with increasing y since the highest frequency modes dissipate faster, a conclusion which agrees with Figure 10. In our simulation, the free-stream velocity field is quasi two-dimensional, since fluctuations of the spanwise component, w', are very small by comparison to u' and v'. Instantaneous contours of fluctuating u' show that the largest structures of the flow are arranged in alternating bands that occupy the entire span of the numerical domain, as seen in Figure 11.

Figure 12 shows that, at an equal distance $y/H = 4.7$ from the wall, peak magnitudes in the cube simulation's span-wise averaged streamwise spectra increase with downstream distance, but the peak frequency does not change. This suggests that the free-stream fluctuations created by the cube may propagate downstream and upwards. This effect could be associated with the boundary layer thickness growth, but the value of the energy spectra peak measured at $x = 20H, y = 4.7H$, located at $2.3H$ from the boundary layer edge, is lower than the peak value measured at $x = 45H, y = 6.5H$, at $2.9H$ from the boundary layer edge. The frequency of the peak is very low and cannot be associated directly with the vortex shedding of the cube measured closer to the wall. Note that in previous experimental studies of round and square cylinders (Porteous et al., 2014), a low-frequency peak ($St = 0.07$, associated to the tip flow, in addition to the vortex shedding peak with $St \approx 0.15 - 0.2$) was only visible in the far-field spectra of cylinders with high aspect ratio ($H/W > 9$), where W is the cylinder width), which is not the case here.

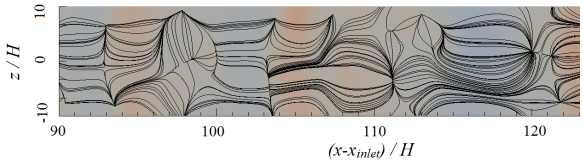

Figure 11: Unperturbed boundary layer: Instantaneous contours of fluctuating streamwise velocity and planar streamlines, in the plane $z = 6H$ ($u' = [-0.05, 0.05]$).

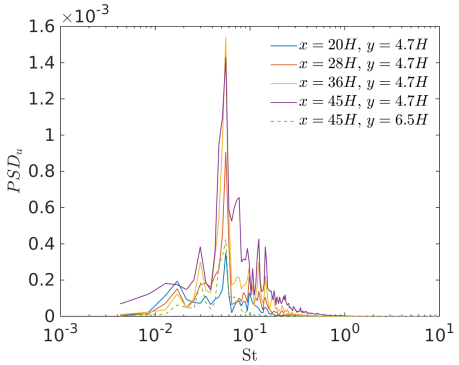

Figure 12: Span-averaged streamwise spectra, from the cube simulation, measured in the free-stream at several streamwise positions (points $A - D$ and D').

Instantaneous velocity contours of the simulation with the cube (Figure 13, at an arbitrary $t_0 = 750H/U_\infty$) are very similar to those found in the unperturbed ZPG boundary layer, and they are also dom-

inated by the pattern mentioned above. Then, simple visualisations of these planes are not helpful for identifying potential differences and explain the spectral peak observed in Figure 10. However, Figure 14 shows evident differences in the velocity signal at $x = 45H$, $y = 6H$, $z = 0$ between the two simulated flows, The time-signal from the immersed-cube simulation presents higher maxima and minima and the separation between these peaks is relatively constant over time. This suggests that the cube is enhancing free-stream fluctuations at a particular frequency, consistent with the peak location in the energy spectra. To confirm this, the probability distribution function (PDF) of the time-lapse between maxima of u' (conditioned to $u' > 2 \cdot 10^{-3}$) was computed at $x = 45H$, $y = 6H$. This PDF shows that the events with $\Delta t \approx 20H/U_\infty$, equivalent to the frequency $St = 0.05$, have a high probability peak of approximately 8% when the cube is present (Figure 15). The PDF of the time-lapse between local minima (conditioned to $u' < -2 \cdot 10^{-3}$) do not show such high peaks at $\Delta t \approx 20H/U_\infty$, supporting existing evidence of high skewness in the velocity signal at this location.

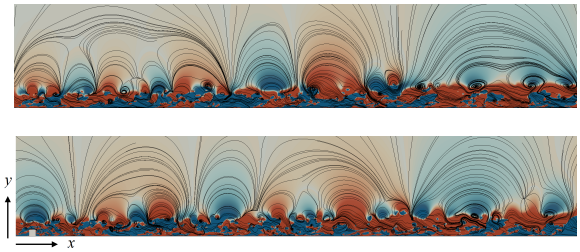

Figure 13: Instantaneous contours of fluctuating streamwise velocity ($u' = [-0.01, 0.01]$) along planar streamlines, in the plane $z = 0$. Upper figure: unperturbed boundary layer, lower figure: cube inmersed in the boundary layer. Taken at an arbitrary time $t_0 = 750H/U_\infty$.

Investigation on the origin of the far-field peak

In order to investigate the origin of the mechanism responsible for the modulation of the free-stream velocity, an additional simulation was performed to analyse the cube flow-field under laminar conditions, at Reynolds $Re_H = 750$. A 3-D array of virtual probes where placed around the solid cube in a smaller simulation with $357 \times 96 \times 128$ cells and domain size equal to $35 \times 15 \times 8H$. The boundary conditions were kept the same as in the turbulent simulation, but the incoming boundary layer ($\delta \approx H$) was set to a laminar Blasius profile, in order to focus on the coherent structures generated by the cube.

Instantaneous visualisations of vortices using the λ_2 criterion (Jeon and Hussain, 1995) are presented in Figure 16 and suggest that the main structure responsible for the unsteady modes is a hairpin vortex generated at the top of the cube. The two upper side edges induce vortical motions, which presumably interacts with the shear layer created over the cube and

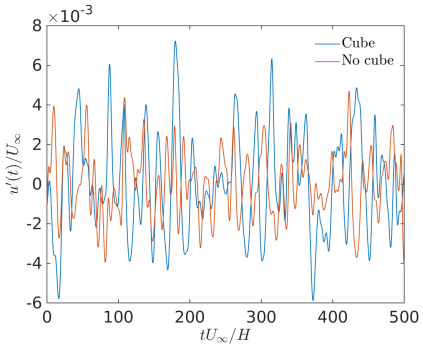

Figure 14: Time signal of the fuctuating streamwise velocity u', with and without the cube, at the position $x = 45H$, $y = 6H$.

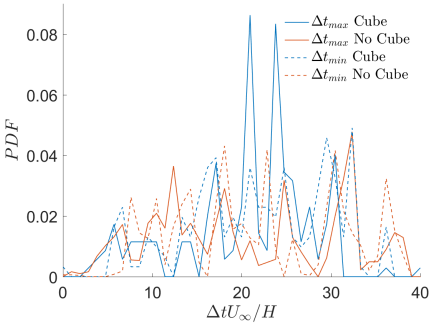

Figure 15: Probability distribution function of the time lapse between velocity maxima (conditioned to $u' > 0.002$) and minima (conditioned to $u' < -0.002$), at the position $x = 45H$, $y = 6H$, $z = 0$.

leads to flow instability. This mechanism creates a primary street of symmetric hairpin vortices, which are detached from the wall. In the laminar case, vortex generation occurs around $x_{vg} = 5H$ from the rear wall, further downstream than under turbulent conditions ($x_{vg} \approx 0$). The contours of λ_2 suggest that two secondary streets of hairpin vortices, attached to the wall, are generated on the sides of the primary structures, as a possible result of the interaction between these ones and the wall.

The Strouhal number associated to the vortex structures is $St = 0.22$, higher that the shedding frequency reported for the turbulent case. This unsteady mode appears as a sharp and intense peak in the energy spectra, which is shown for different downstream locations in Figure 17. The peak intensity is maximum around $x = 5H$, $y = H$ from the cube, right after the shear layer becomes unstable. When moving downstream at $y = H$, $z = 0$, the peak intensity is reduced, but it can be still detected up to the domain outlet, since there is no interaction with boundary layer turbulence. Starting from around $x/H = 15 - 20$, a secondary peak, with lower Strouhal number $St \simeq 0.05$, becomes noticeable in the energy spectra, and its magnitude increases further downstream. At $x/H = 15$ to 28,the peak magnitude is of the same order as the peak

at $St = 0.22$. The potential source of this peak may be the de-alignment between primary and secondary vortex streets, which can create a low frequency modulation of the velocity fluctuations. This de-alignment could be caused by the different convection velocity of the attached and detached hairpin vortices. Therefore, this phenomenon may explain the peak found in far-field spectra of the cube immersed in a TBL, as the Strouhal number is the same in both cases.

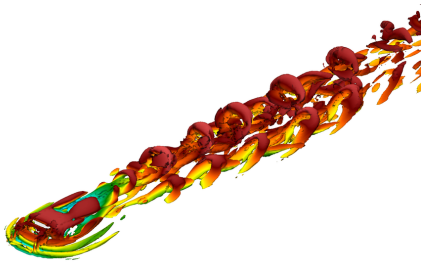

Figure 16: Vortex visualisation in the laminar simulation using λ_2 criterion. Threshold of $\lambda_2 = -0.04$. Coloured by streamwise velocity

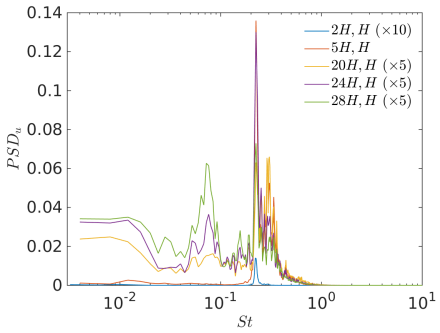

Figure 17: Energy spectra of streamwise velocity u at different positions x, y, from the cube laminar simulation ($Re_H = 750$).

4 Conclusions and further work

The interaction between a boundary layer and a wall-attached cube generates a low-frequency sharp peak in the far-field energy spectra which persists for long downstream distances with a constant Strouhal number $St = 0.05$. This peak is not probably due to numerical effects nor related to the background boundary layer turbulence, since it was not identified in the unperturbed zero-pressure gradient TBL. The source of this tonal peak has been further investigated, since the Strouhal number does not correspond to the vortex shedding detected close to the cube with $St = 0.14$, and this tonal peak might be associated to an additional phenomenon. A laminar simulation to investigate the coherent structures created by the cube, at $Re_H = 750$, revealed that there are two distinct vortex streets. The interaction or de-synchronisation between these two periodic structures may generate the peak with $St = 0.05$, which was also present in the spectra of this simulation at $x > 20H$. Future work can extend this study to different cube heights to analyse the effect of the aspect ratio on the far-field spectra. The interaction between two cubes will be investigated, as well as the placement of fractal and regular grids downstream of the cube, as possible mechanisms to reduce or suppress the low-frequency peak (Laizet et al., 2012).

Acknowledgments

The investigations presented in this paper have been obtained within the European research project Multisolve, granted by the European Comission framework Marie Curie. We would like to aknowledge the use of the following HPC facilities: SuperMUC, thanks to PRACE; ARCHER, supported by UKTC with EPSRC grant number EP/L000261/1; and Blue-Joule, supported by the Hartree Centre.

References

Castro, I.P. and Robins, A.G., The flow around a surface-mounted cube in uniform and turbulent streams, J. Fluid Mech., 79(2):307-335, 1977

Jeong, J. and Hussain, F., On the Identification of a Vortex. J. Fluid Mechanics, 285:69-94, 1995.

Laizet, S. and Lamballais, E., High-order compact schemes for incompressible flows: a simple and efficient method with the quasi-spectral accuracy, J. Comp. Phys., 228(15): 5989-6015, 2009

Laizet, S., Fortuné, V., Lamballais, E. and Vassilicos, J. C. Low Mach number prediction of the acoustic signature of fractal-generated turbulence. Int. J. Heat Fluid Flow, 35:25-32, 2012

Martinuzzi, R.J. and Tropea, C., The Flow Around Surface-Mounted, Prismatic Obstacles Placed in a Fully Developed Channel Flow. J. Fluids Eng., 115:85-92, 1993

Martinuzzi, R.J. and Havel , B., Vortex shedding from two surface-mounted cubes in tandem, Int. J. Heat Fluid Flow , 25(3):364- 372, 2004

Meinders E.R, Hanjalic, K. and Martinuzzi, R.J., Experimental Study of the Local Convection Heat Transfer From a Wall-Mounted Cube in Turbulent Channel Flow, J. Heat Transfer, 121(3):564-573, 1999

Philips, O. M., The irrotational motion outside a free turbulent boundary, Math. Proc. Cambridge Phil. Soc. 51:220-229, 1955

Porteous, R., Moreau, D. J. and Doolan, C., A review of flow-induced noise from finite wall-mounted cylinders, J. of Fluids and Struc., 51: 240-254, 2014

Schlatter, P. and Örlü R., Turbulent boundary layers at moderate Reynolds numbers: inflow length and tripping effects. J. Fluid Mech., 710:5-34, 2012

Vinuesa, R. Schlatter, P., Malm, J., Mavriplis C. and Henningson, D.S., Direct numerical simulation of the flow around a wall-mounted square cylinder under various inflow conditions, J. Turbulence, 16(6): 555-587, 2015

Wang, H.F., Zhou, Y. and Mi, J., Effects of aspect ratio on the drag of a wall-mounted finite-length cylinder in subcritical and critical regimes, Experiments in fluids, 53(2): 423-436, 2012

Yakhot, A., Liu, H., and Nikitin, N., Turbulent Flow around a wall-mounted cube: A direct numerical simulation. Int. J. Heat Fluid Flow, 27:994-1009, 2006